Rock Mechanics Bulletin 5 (2026) 100244

Contents lists available at ScienceDirect

Rock Mechanics Bulletin

journal homepage: www.keaipublishing.com/en/journals/rock-mechanics-bulletin

The frictional sliding properties of antigorite gouge under hydrothermal conditions

Shimin Liu[a, b], Mengke An[c], Wenhao Dai[b, d, *], Huiru Lei[b], Lei Zhang[b], Yongsheng Zhou[b], Zekang Yang[b]

[a] School of Fire Protection Engineering, China People's Police University, Langfang, 065000, China
[b] State Key Laboratory of Earthquake Dynamics and Forecasting, Institute of Geology, China Earthquake Administration, Beijing, 100029, China
[c] Department of Civil and Environmental Engineering, The Hong Kong Polytechnic University, Hong Kong, 100872, China
[d] Jiangxi Earthquake Agency, Nanchang, 330026, China

ARTICLE INFO

Keywords:
Antigorite
Friction coefficient
Velocity dependence
Steady sliding
Pore fluid pressure

ABSTRACT

As a weak mineral overlying subduction-zone faults, the widespread presence of antigorite can markedly affect subduction-zone dynamics. To better understand the mechanical properties of antigorite-bearing faults, we conducted frictional sliding experiments on antigorite under hydrothermal conditions. The experimental setup involved a constant confining pressure of 100 MPa, a low pore fluid pressure of 30 MPa, and temperatures ranging from 100 °C to 500 °C. We varied the axial loading rate between 0.04, 0.2, and 1.0 μm/s to examine the velocity dependence of the friction coefficient. The results showed that the friction coefficient of antigorite exhibited a significant temperature dependence. Between 100 °C and 400 °C, the friction coefficient decreased from 0.66 to 0.54 as the temperature increased. Above 400 °C, the friction coefficient increased, reaching 0.7. The velocity dependence of antigorite exhibited velocity strengthening ($a - b > 0$) throughout the entire experimental temperature range (100 °C–500 °C). The impact of pore-fluid pressure on the frictional behavior of antigorite was also significant. Under low pore-fluid pressure (30 MPa), the frictional strength increases above 400 °C, associated with dehydration hardening. In contrast, at high pore fluid pressure, frictional weakening continues at elevated temperatures, indicating that pore fluid pressure plays a crucial role in regulating the frictional stability of antigorite. Our experimental results demonstrate that the pore fluid pressure plays a key role in regulating the temperature-dependent frictional behavior of antigorite, highlighting the need for further investigation under varying fluid pressure conditions.

1. Introduction

Serpentine is a hydrous, magnesium-rich silicate mineral whose formation is closely linked to the hydrothermal alteration of ultramafic rocks. It is widely distributed in tectonic environments, such as convergent faults, subduction zones (Christensen, 1972), and the mantle wedge (Hacker et al., 2003; Hilairet et al., 2007), with its formation process strongly influenced by plate subduction dynamics. In subduction zone of tectonic plates, metamorphic dehydration of hydrous minerals generates substantial fluids (Peacock, 1990). As these fluids migrate to the Moho depth beneath the forearc mantle, where they interact with pyroxene and olivine, undergoing retrograde metamorphic reactions and forming a serpentine-dominated hydrous mineral assemblage (Peacock, 1993; Kawakatsu and Watada, 2007). Experimental studies show that serpentine exhibits a significantly lower frictional strength compared to crustal lithifying minerals (Reinen et al., 1991; Moore et al., 1997). Brune et al. (1969) and Zoback (1987) further revealed that serpentine's low-strength properties could stabilize faults and promote creep, influencing the dynamic evolution of subduction zones. Given serpentine's critical role in subduction zones, numerous scholars have explored its genesis mechanisms and dynamic characteristics after Dietz and Raleigh et al. (Dietz, 1963; Raleigh and Paterson, 1965; Takahashi et al., 2011). These studies have deepened the understanding of serpentine's formation and provided important theoretical foundations for examining its effects on seismic activity, plate coupling, and other geological processes.

* Corresponding author.
E-mail address: daiwh19@163.com (W. Dai).

Peer review under the responsibility of Chinese Society for Rock Mechanics & Engineering.

https://doi.org/10.1016/j.rockmb.2025.100244
Received 13 June 2025; Received in revised form 23 July 2025; Accepted 29 August 2025
Available online 1 September 2025

Serpentine minerals are trioctahedral 1:1 phyllosilicate with the ideal composition $Mg_3Si_2O_5(OH)_4$. Their structures consist of a continuous SiO_4 tetrahedral sheet bonded to a $Mg(OH)_2$ octahedral sheet. Mismatched lattice parameters between the two sheets impose curvature and give rise to three polytypes, i.e., lizardite (flat layers), chrysotile (cylindrical layers rolled into fibres) and antigorite (modulated layers with periodic reversals of curvature) (Evans, 2004; Schwartz et al., 2013). The interlayer interaction forces primarily consist of hydrogen bonds, electrostatic interactions, and structural water. Additionally, all polytypes share (001) basal planes separated by ~7.2 Å. Antigorite differs from lizardite/chrysotile by a periodic inversion of layer curvature every m tetrahedral repeat, producing a "corrugated" or wave-like topology. The general formula may be written $Mg_{3m-3}Si_{2m}O_{5m}(OH)_{4m-6}$ and the m-values are commonly 17, 31 or 44 (Evans, 1976; 2004). The key characteristics are as follows. Firstly, the narrow interlayer spaces, with water primarily existing as structural OH groups. Secondly, the (001) plane remains the weakest cleavage, but the wavy morphology promotes easier activation of secondary slip planes such as [101]. Lastly, it is stable under high-pressure and high-temperature conditions, allowing it to transport water into deep subduction zones.

The geophysical significance of antigorite is reflected in three main aspects: (1) its high water content, (2) the strong crystallographic preferred orientation formed during shear deformation, and (3) dehydration processes occurring under specific temperature and pressure conditions. These characteristics provide crucial mineralogical evidence for explaining low seismic velocity anomalies, slow slip phenomena, and strong anisotropy observed in the mantle wedge above subducting plates (Katayama et al., 2009; Jung, 2011; Okazaki and Katayama, 2015; Liu et al., 2023; Li et al., 2025).

In recent years, the debates over whether serpentine dehydration triggers intermediate-depth earthquakes have intensified (Raleigh and Paterson, 1965; Jung and Green, 2004; Chernak and Hirth, 2010). Since Raleigh and Paterson (1965) proposed the "dehydration embrittlement" theory, it has been used to explain the origin of intermediate-depth earthquakes. According to the theory, low-permeability serpentinite increases pore pressure during dehydration, significantly reducing rock fracture strength. Jung and Green (2004) observed dehydration products (forsterite) oriented along brittle fault zones under unstable temperature and pressure conditions for antigorite, supporting the brittle instability mechanism. However, Chernak and Hirth (2010) conducted similar experiments under higher temperature and pressure conditions (1.5 GPa/700 °C), finding a deformation mode dominated by ductile diffusion creep. These conflicting experimental results indicate that the rheological behavior of serpentinite in subduction zones is highly complex, with its mechanical response controlled by both mineral phase transitions and tightly coupled with microstructural evolution, fluid migration, and other multiscale processes. Therefore, the specific impact of serpentine on intermediate-depth earthquakes remains widely debated.

Extensive researches have been conducted on the frictional properties of serpentine minerals. For example, Takahashi et al. (2011) highlighted that in impermeable serpentinite faults oriented within a specific direction in a regional stress field, pore water pressure can significantly influence both fault strength and stability. At lower pore fluid pressures (10–20 MPa), several experimental studies have shown a positive correlation between the friction coefficient of antigorite and temperature. Moore et al. (1997) observed that, under 10 MPa pore fluid pressure, 110 MPa confining pressure, and temperatures ranging from 25 °C to 194 °C, the friction coefficient increased from 0.45 to 0.5 as temperature rose, displaying stable velocity strengthening. Later, Moore and Lockner (2007) extended the temperature range to 400 °C, finding that the friction coefficient increased to 0.6. Similarly, Okazaki and Katayama (2015) observed that under 20 MPa pore fluid pressure and high temperatures (400 °C–650 °C), the friction coefficient of antigorite increased from 0.56 to 0.66, further confirming this trend. Notably, when pore fluid pressure increased to 50 MPa, the temperature's influence on the friction coefficient reversed. Under 100 MPa effective normal stress and temperatures between 200 °C and 350 °C, Moore and Lockner (2013) conducted experiments using granite as the driving blocks and found that the friction coefficient decreased with increasing temperature, dropping significantly from 0.6 to 0.3. They suggested that this temperature weakening effect might be linked to the dissolution-transport creep mechanism facilitated by pore fluids, highlighting the role of fluid-rock interactions in regulating frictional behavior.

Previous studies have also investigated the behavior of serpentine under higher pore fluid pressure conditions. Liu et al. (2023) conducted friction experiments under 100 MPa pore fluid pressure, 30 MPa effective normal stress, and temperatures between 100 °C and 500 °C. They found that within this temperature range, the friction coefficient of antigorite decreased systematically with increasing temperature, and that under high porefluid pressures serpentine may play a critical modulating role in triggering slow earthquakes along subduction zones.

In summary, variations in pore-fluid pressure markedly affect both the frictional strength and stability of antigorite fault. However, the specific mechanisms of pore fluid pressure under varying temperature and pressure conditions require further investigation. We have previously explored the frictional behavior of antigorite at high pore-fluid pressure (P_f = 100 MPa). To enable clearer comparison and to better evaluate the influence of pore-fluid pressure on serpentine's frictional properties, the present experiments were carried out at a pore-fluid pressure of 30 MPa.

Based on this background, we carried out hydrothermal shear experiments using antigorite as the gouge material. The specific conditions were a confining pressure of 100 MPa, a pore fluid pressure of 30 MPa, and temperatures ranging from 100 °C to 500 °C. To examine the response of friction to changes in sliding rate and its effect on sliding stability, the shearing rate was switched between 0.04 and 1.0 μm/s.

2. Materials and methods

2.1. Experiment materials

Antigorite samples were collected from Hada Bei Town, Xiuyan County, Liaoning Province, China (40°28′31″N, 123°0′48″E). The samples were manually ground, crushed, and sieved through a 200-mesh screen to control particle size. Gabbro cylinders with a diameter of 20 mm and a length of 40 mm were used as the driving blocks in the experiment. The driving blocks had a saw cut inclined at a 35° to the axial direction. To ensure uniform pore fluid pressure, the upper driving block had a dual-pore design, while the lower section was made of intact driving blocks to prevent pore pressure loss. To control the roughness of the pre-cut surface, 200-mesh sandpaper polished it before the experiment. After polishing, a 1 cm-thick layer of antigorite gouge was evenly spread on the surface.

2.2. Experimental apparatus and procedure

The experiment was conducted using a high-temperature, high-pressure triaxial apparatus with argon gas as the medium. Argon gas was used for pressurization, and a servo control system maintained a constant confining pressure with an accuracy of ±0.5 MPa throughout the experiment. A servo-controlled pore water pressure system also maintained the pore water pressure within ±0.3 MPa. The YAMATAKE DC30 temperature control system ensured uniform temperature distribution along the sample section under high-temperature convective conditions, with fluctuations kept within ±13 °C.

The schematic diagram of the experimental apparatus is shown in Fig. 1. The entire assembly, including driving blocks, tungsten carbide end-pieces, and alumina pistons, was encapsulated in a 0.35 mm-thick annealed copper tube. To ensure uniform heat transfer and prevent thermal convection, boron nitride powder filled the space between the

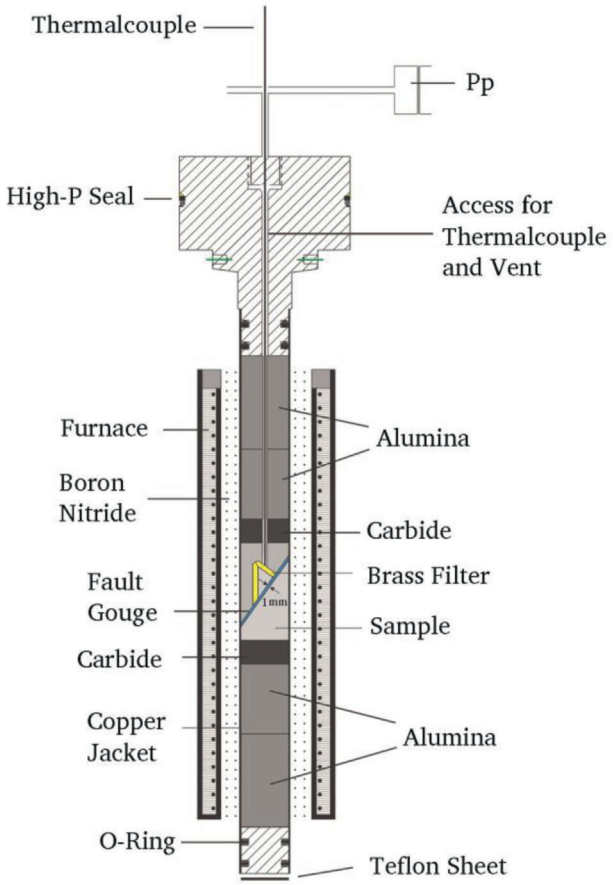

Fig. 1. Sketch of the sample assembly.

copper tube and the heating furnace. The specific details regarding sample preparation have been described in detail in the published article (He et al., 2007) and will not be elaborated here.

After assembling the sample, it is placed into a high-pressure vessel, sealed, and the confining pressure is applied to around 100 MPa with servo control. Then, the pore fluid pressure is applied to approximately 30 MPa with servo control. The temperature is increased to the required experimental temperature and maintained stable by the temperature control system. The confining pressure and pore pressure are further adjusted to stabilize at 100 MPa and 30 MPa, respectively. Next, the axial pressure is applied to set the loading rate. The experiment begins with a loading rate of 1.0 μm/s until the curve reaches a steady state, after which the rate is switched. To obtain the velocity dependence of the frictional strength, the loading rate is switched between 0.04, 0.2, and 1.0 μm/s, with each step corresponding to a 0.2 mm displacement. The data sampling frequency is set to 1 Hz. During data processing, the experimental mechanical data were corrected for pressure changes due to variations in contact area during shear and for the shear strength of the copper tube. The correction methods are detailed in He et al. (2006, 2007).

2.3. Acquisition of frictional constitutive parameters

The rate-and-state friction constitutive relationship (RSF), based on experimental research, is widely accepted as a theoretical framework for describing the frictional sliding behavior of rocks (Dieterich, 1979; Ruina, 1983). This equation provides a macroscopic description of frictional sliding behavior. Within this framework, the general friction coefficient is described as a function of velocity V and state θ, i.e.,

$$\mu = \mu_* + a\ln(V/V_*) + b\ln(\theta/\theta_*) \tag{1}$$

here, V^* represents the reference rate, and μ^* denotes the steady-state friction coefficient at the reference rate V^*. a and b are the velocity-dependent and state-dependent constants of the friction coefficient, respectively. The parameter a characterizes thermally activated creep behavior following an exponential (Arrhenius-type) dependence, representing a dominant deformation mechanism under low-temperature and high-stress conditions where dislocation glide governs plastic flow (Nakatani, 2001). The parameter b quantifies the evolution effect, which exclusively correlates with deformation mechanisms that induce increases in microscale granular contact area. In the equation, the state variable θ has a time dimension, representing the average contact time between the asperities of two frictional surfaces at a given rate. The second term, $a\ln(V/V^*)$, represents the instantaneous response of the friction coefficient to changes in sliding velocity. The third term, $b\ln(\theta/\theta^*)$, describes the evolution of the friction coefficient with respect to the state variable θ. When the rate is constant and the state variable evolves to a steady value, the friction coefficient reaches its steady-state value, expressed as,

$$\mu_{ss} = \mu_* + (a-b)\ln\left(\frac{V}{V_*}\right) \tag{2}$$

The differential form of Eq. (2) after the change from rate V_1 to V_2 is as follows:

$$a - b = \frac{\Delta\mu^{ss}}{\ln(V_2/V_1)} \tag{3}$$

μ represents the coefficient of friction, and the superscript "ss" indicates the steady-state value at any sliding velocity V. V_1 and V_2 represent the loading rates before and after the velocity step, respectively. The term $(a-b)$ is an important parameter describing the stability of frictional sliding, known as the velocity dependence parameter. When $(a-b) > 0$, the steady-state friction coefficient is positively correlated with sliding velocity, known as velocity strengthening; conversely, when $(a-b) < 0$, it is velocity weakening. The sign of $(a-b)$ is influenced by various factors, including gouge type, temperature, normal stress, and pore fluid, with their effects being interdependent. For faults in continuous media, under stable tectonic loading, unstable sliding nucleation occurs only when velocity weakening happens (Tse, 1986; Dieterich, 1992). Since velocity weakening is directly related to unstable sliding nucleation on faults, measuring the "velocity dependence" of rock friction strength in laboratory experiments can predict the conditions under which a fault may experience an earthquake. This study explores the frictional sliding characteristics of antigorite, based on the rate-and-state friction constitutive relationship, focusing on how its friction coefficient and the frictional sliding stability parameter $(a-b)$ change with temperature and loading rate.

2.4. XRD and SEM methods

The X-ray diffraction (XRD) analyses were performed using a Bruker D8 AD-VANCE X-ray diffractometer with Cu Kα radiation at the State Key Laboratory of Earthquake Dynamics, Institute of Geology, China Earthquake Administration, Beijing, China. Data were collected over a 2θ range of 5°–70° with a step size of 0.02°, and the database used for analysis was ICDD-PDF-4. The microstructures of the antigorite samples were analyzed using a Zeiss Sigma scanning electron microscopy (SEM). The backscatter electron images (BSE) and chemical compositions of minerals in the antigorite samples were obtained at the operating conditions including an accelerating voltage of 15 kV and a working distance of 8.5–8.7 mm.

3. Results

3.1. XRD results

The mineralogical composition of the experimental samples was characterized by X-ray diffraction (XRD). As shown in Fig. 2, the diffraction pattern is dominated by antigorite (ICSD PDF #00-007-0417). And Fig. 2 shows the most intense peaks. Minor reflections at $2\theta = 30.9°$ and 32.9° are assigned to dolomite (ICDD #01-075-1655) and magnesite (ICDD #01-080-0042), respectively, consistent with petrographic observations.

3.2. Mechanical properties

This study conducted a series of frictional sliding experiments on antigorite gouge under a confining pressure of 100 MPa and a pore fluid pressure of 30 MPa. The friction coefficient-displacement curves for antigorite gouge are shown in Fig. 3. The characteristics of the curves under these control conditions are as follows. In the temperature range of 100–300 °C, the friction coefficient of antigorite decreases slightly. At 400 °C, the shear strength of antigorite shows strong slip weakening after reaching its peak. At 500 °C, a minor slip weakening phenomenon is observed, but it is significantly weaker than at 400 °C. Additionally, within the temperature range of 100–500 °C, velocity strengthening and steady sliding are observed. The experimental conditions and relevant parameters for this series of experiments are detailed in Table 1.

3.3. Frictional strength

We selected the friction coefficient at an axial inelastic strain displacement of 2 mm and a loading rate of 1.0 μm/s to examine the relationship between temperature and frictional strength. The results, shown in Fig. 4, indicate that within the experimental temperature range, the friction coefficient of antigorite initially decreases and then increases with temperature. In the temperature range of 100–400 °C, the friction coefficient decreases from 0.66 to 0.54. However, as the temperature reaches 500 °C, the friction coefficient of antigorite begins to rise, reaching 0.7.

3.4. Friction stability parameter (a – b)

Fig. 5 shows the velocity dependence parameter ($a - b$) of antigorite

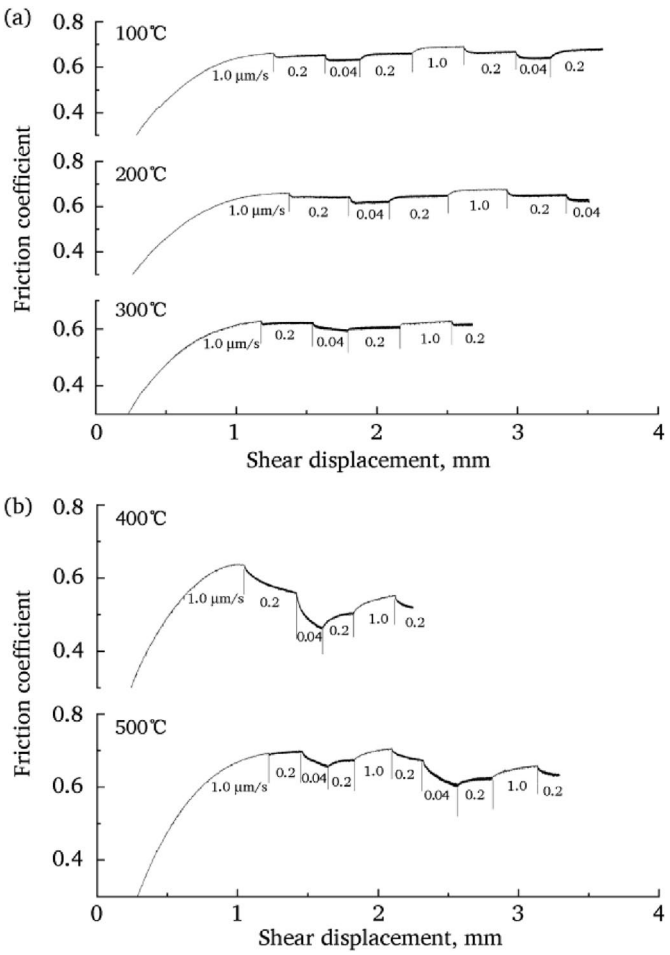

Fig. 3. Friction coefficient of antigorite gouge plotted as functions of displacement under temperature condition of (a)100–300 ℃ and (b) 400–500 ℃.

frictional sliding as a function of temperature. Under hydrothermal conditions, the velocity dependence of antigorite exhibits velocity strengthening characteristics ($a - b > 0$) across the entire experimental temperature range. Within the temperature range of 100–300 °C, its

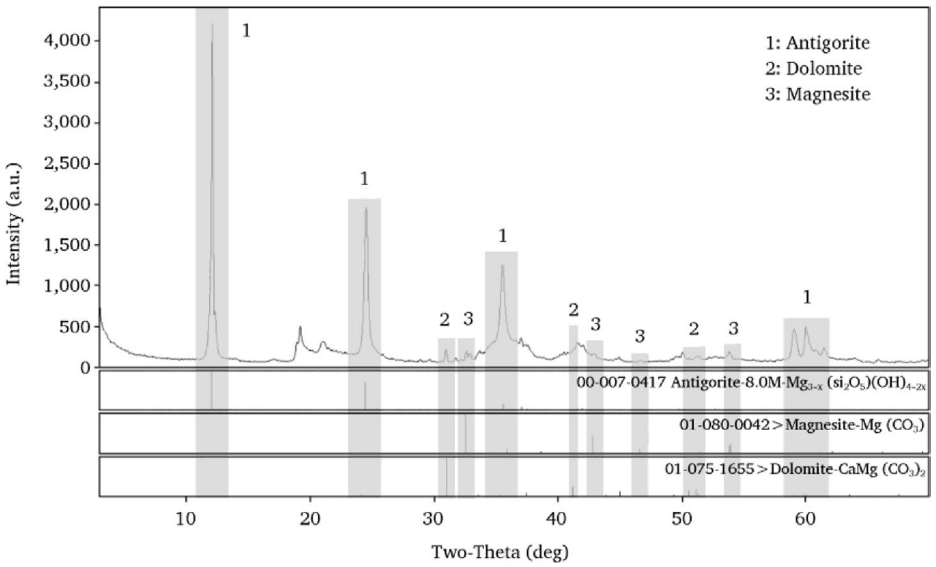

Fig. 2. The X-ray diffraction pattern for the antigorite.

Table 1
Experimental conditions and results of antigorite gouge under hydrothermal conditions.

Sample	T/(°C)	C_p/MPa	P_f/MPa	μ	$a-b$	a ($\times 10^{-2}$)	b ($\times 10^{-4}$)	Mode of motion
Atg-30-1	100	100	30	0.659	0.0181	1.83	1.833	Steady slip
Atg-30-2	200	100	30	0.643	0.0173	1.75	1.746	Steady slip
Atg-30-3	300	100	30	0.606	0.0093	0.94	0.935	Steady slip
Atg-30-4	400	100	30	0.543	0.0114	1.14	1.136	Steady slip
Atg-30-5	500	100	30	0.701	0.0100	1.01	1.011	Steady slip

T: temperature at the top of the driving block.
μ: steady-state friction coefficient at an axial displacement of 2.0 mm and a loading rate of 1.0 μm/s.
$a-b$: average of the velocity dependence calculated from multiple rate steps (1.0–0.2–0.04 μm/s).
C_p: confining pressure.
P_f: pore-fluid pressure.
d_c values derived by data fitting are 1 μm for stable sliding cases.

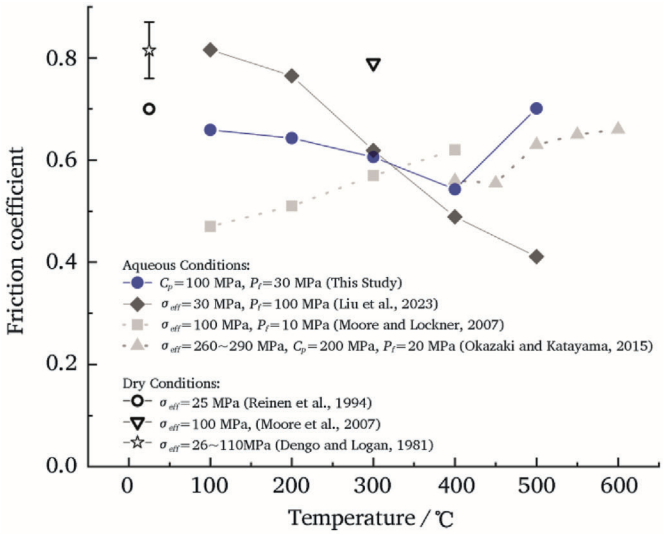

Fig. 4. Friction coefficient of antigorite gouge plotted against temperature (σ_{eff} is effective normal stress, C_p is confining pressure, P_f is pore fluid pressure).

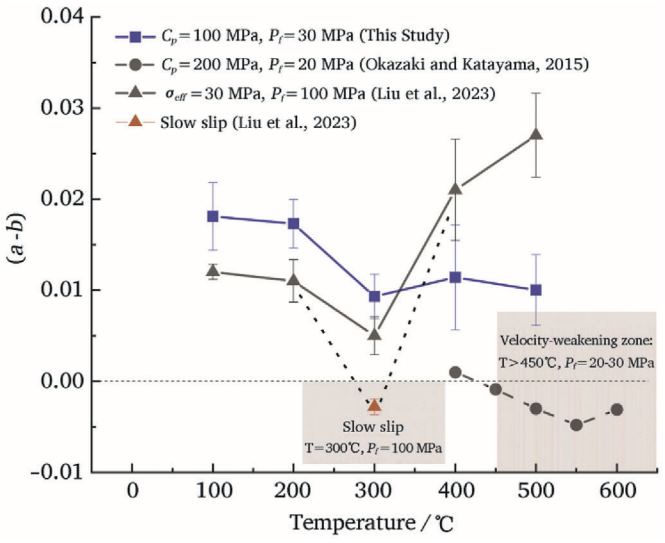

Fig. 5. Velocity dependence value ($a-b$) of antigorite gouge plotted against temperature (σ_{eff} is the effective normal stress, C_p denotes the confining pressure, P_f denotes the pore-fluid pressure).

velocity dependence gradually weakens. Due to the occurrence of slip-hardening or slip-weakening behavior in the mechanical curves, the selected mechanical data was detrended before further analysis. Notably, under sustained thermal exposure exceeding 300 °C, the parameter ($a-b$) exhibits a non-monotonic response, characterized by an initial increase followed by a progressive decline. Throughout this process, the velocity dependence is lowest at 300 °C.

3.5. Microstructural features

In this study, scanning electron microscopy (SEM) was employed to examine thin sections of deformed gouge cut along the sample axis and shear direction, with the aim of elucidating the deformation mechanisms of antigorite at different temperatures. Given the variation in frictional strength of antigorite with temperature, samples at 200 °C and 500 °C were selected for microstructural shear texture studies. Meanwhile, to better understand the microstructural results, we explored the deformation mechanisms of antigorite in the shear zone through crystallochemical analysis.

At 200 °C, the microstructural features of the deformed gouge are characterized by localized Riedel (R) shears and Boundary (B) shears (Fig. 6a). The B shear is continuous along the gouge-wall rock interface. The Riedel shears were not fully developed (Fig. 6a), and significant grain size reduction of the gouge particles was observed in the localized shear zones. From a crystallochemical perspective, at this temperature (200 °C), strong hydrogen bonding and the corrugated stacking of antigorite's 1:1 layers inhibit intracrystalline slip along the basal (001) planes, forcing the gouge to accommodate shear by brittle mechanisms (i.e., micro-fracturing and grain boundary sliding). In this regime, antigorite generates little to no dislocation glide because the thermal energy is insufficient to overcome the interlayer hydrogen bonds, and thus the shear localization (R and B shears) and grain size reduction dominate the deformation.

At 500 °C, the antigorite gouge generally exhibits diffuse shear deformation, with underdeveloped localized shear deformation. However, the shape-preferred orientation of gouge particles observed locally (Fig. 7a) indicates that under these conditions, the antigorite gouge predominantly undergoes generalized shear deformation. Additionally, the observations reveal that antigorite particles exhibit a certain degree of brittle fracturing and granulation (Fig. 7b). However, the extent of granulation is notably less pronounced than that observed in samples subjected to 200 °C conditions (Figs. 6a and 7a). This suggests that at elevated temperatures of around 500 °C, plastic deformation mechanisms become activated, which in turn accommodate part of the imposed shear deformation. From a crystallochemical perspective, at this temperature (500 °C), the thermal activation is sufficient to initiate plastic deformation via dislocation glide on the basal planes where bonding is weakest. We infer that antigorite gouge at this temperature engages slip systems with Burgers vectors lying in the (001) plane (for example, along the [010] direction, as suggested by the observed shape-preferred orientation of grains), producing intracrystalline slip bands that accommodate distributed shear. The motion of these dislocations entails the breaking and reformation of O–H…O hydrogen bonds

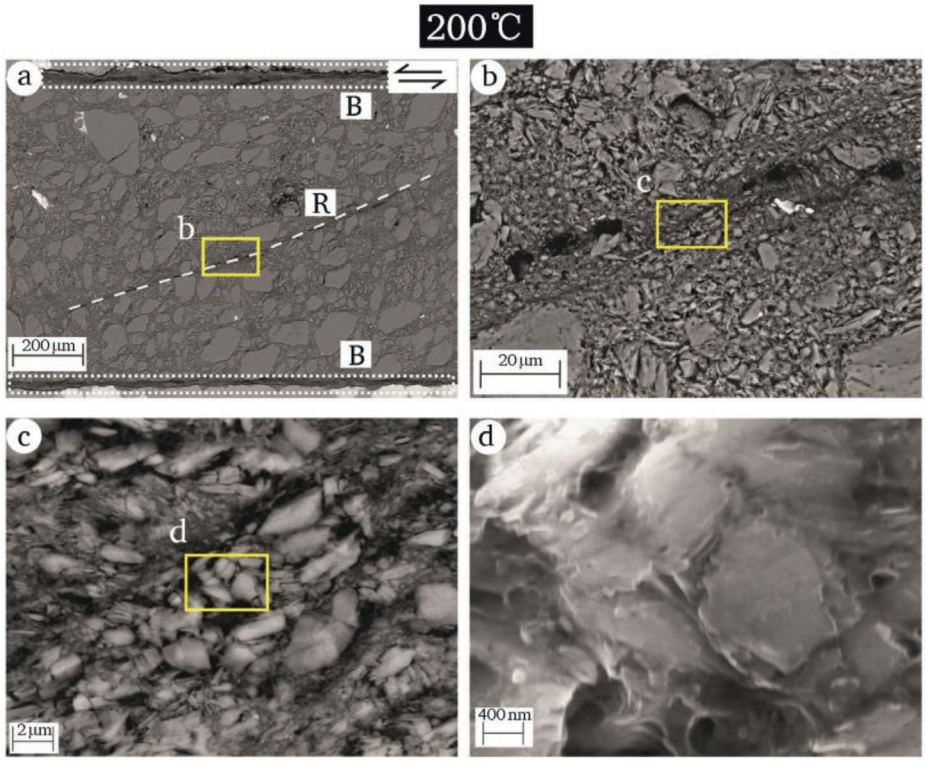

Fig. 6. Backscattered electron images (BSE) and secondary electron images (SE) of samples sheared at a temperature of 200 °C. Panels (b) and (c) are BSE images, while (d) is SE image. The SE images, captured in InLens mode, predominantly collect low-energy secondary electrons from the surface of the samples, making them excellent for revealing fine surface details. B denotes Boundary shear; R represents Riedel shear.

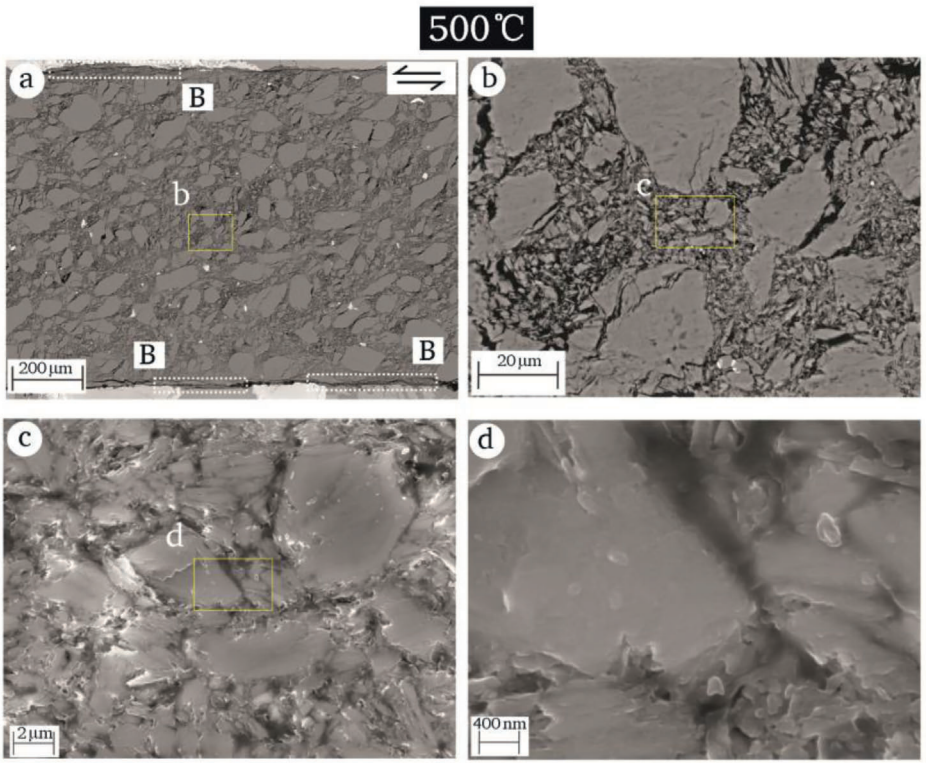

Fig. 7. Backscattered electron images (BSE) and secondary electron images (SE) of samples sheared at a temperature of 500 °C. Panels (b) and (c) are BSE images, while (d) is SE image. The SE images, captured in InLens mode, predominantly collect low-energy secondary electrons from the surface of the samples, making them excellent for revealing fine surface details. B denotes Boundary shear.

between layers an energetically easier process than breaking the covalent Si–O bonds in the tetrahedral sheets thus making basal glide the favored mechanism for high-temperature shear in antigorite (Viti et al., 2018).

In summary, the deformation in the shear band evolves from a brittle, frictional sliding mode at 200 °C to a semi-brittle, crystal-plastic mode at 500 °C due to the activation of basal dislocation slip. The associated hydrogen bond rupture and water migration processes fundamentally alter the slip mechanics of antigorite, explaining the observed transition in microstructural textures and the complex temperature-dependent frictional behavior (initial weakening followed by strengthening) of the gouge.

4. Discussion

4.1. Water distribution and migration in antigorite

Fluids exert a pronounced influence on the frictional strength of antigorite gouge. As illustrated in Fig. 4, antigorite gouge exhibits relatively high frictional strength under dry conditions (Dengo and Logan, 1981; Reinen, 1994), whereas the presence of water markedly reduces this strength. This observation aligns with the conclusion of Morrow et al. (2000), who argued that the frictional strength of layered silicates is governed by their capacity to adsorb water (Peacock, 1990).

Antigorite is a water-rich phyllosilicate (~13 *wt*% H_2O) (Wunder and Schreyer, 1997) distinguished by its characteristic modulated, wavy layering. Its ideal composition is expressed as $Mg_{3m\text{-}3}Si_{2m}O_{5m}(OH)_{4m\text{-}6}$. In contrast to smectite, the water in antigorite is not present as free interlayer molecules but is incorporated as structural OH groups (Moore and Lockner, 2013). These hydroxyls reside on the outer surface of the Mg-octahedral sheet and form hydrogen bonds with basal oxygens of the adjacent SiO_4 tetrahedral sheet. Neutron-diffraction and infrared studies (Auzende et al., 2006; French et al., 2019) confirm that these O–H···O hydrogen bonds are critical for interlayer cohesion. Their bond energy is relatively low, about 20–25 kJ mol^{-1}, making them susceptible to thermal activation and shear stress. When such bonds break, proton vacancies are created, allowing water to migrate within the lattice (Hilairet and Reynard, 2009; French et al., 2019). The accompanying removal or redistribution of water weakens interlayer bonding and consequently reduces the mineral's frictional strength (Moore and Lockner, 2007, 2013).

4.2. Frictional properties of antigorite

In this study, antigorite friction experiments were conducted at a pore fluid pressure of 30 MPa, a confining pressure of 100 MPa, and temperatures ranging from 100 °C to 500 °C. The results show a pronounced, temperature-related variation in frictional strength, i.e., the curve exhibits a non-monotonic profile with an inflection point at 400 °C. This pattern indicates the competition and alternation of two distinct temperature-dependent mechanisms.

Between 100 °C and 400 °C, the frictional strength of antigorite gouge decreases steadily with increasing temperature, displaying pronounced thermal weakening that is broadly consistent with observations made under high pore-fluid pressure conditions. Earlier studies have shown that water migration during shear is critical to this behavior (Morrow et al., 2000; Moore and Lockner, 2007). At lower temperatures, water resides as structural OH groups whose O–H···O hydrogen bonds enhance interlayer cohesion and stabilize the layered framework. With progressive heating and continued shear, these hydrogen bonds are progressively broken by thermal and mechanical activation. The resulting proton vacancies then facilitate water diffusion through the lattice (Hilairet et al., 2009). The ensuing reduction in bonding along (001) planes promotes basal slip, lowering shear strength and accounting for the thermal weakening observed in this temperature interval.

When the temperature rises above approximately 400 °C, the frictional behaviour of antigorite gouge changes, i.e., the frictional strength increases sharply, exhibiting clear thermal strengthening. Both the present experiments and previous studies indicate that this transition is linked to dehydration. As antigorite dehydrates, its lattice progressively loses water molecules. This process involves the rupture of O–H···O hydrogen bonds, the creation of proton vacancies, and the nucleation of high-strength forsterite, collectively raising shear strength (Takahashi et al., 2011; Okazaki and Katayama, 2015). The inflection near 400 °C thus marks a shift from a regime dominated by hydrogen-bond weakening to one governed by dehydration hardening. Below 400 °C, the friction decreases with temperature as hydrogen-bond weakening prevails, whereas above 400 °C friction rises abruptly because dehydration hardening becomes the controlling mechanism.

Our results further show that the pore fluid pressure exerts a strong regulatory effect on these competing mechanisms. At a low pore fluid pressure, dehydration proceeds readily and frictional strength increases sharply with temperature. By contrast, at high pore fluid pressure and the elevated fluid pressure suppresses water release and OH breakdown (Perrillat et al., 2005), preserves the hydrogen-bond network, and therefore yields continued thermal and displacement weakening even above 400 °C (Liu et al., 2023). Under these conditions, deformation is controlled mainly by a mixed plastic-brittle response of the antigorite grains rather than by dehydration hardening.

4.3. Impact of different pore fluid pressures on frictional sliding stability of antigorite

Under high pore fluid pressure conditions, the antigorite gouge generally exhibits velocity strengthening behavior across the experimental temperature range. Only at 300 °C and under a loading rate of 0.04 μm/s does it show velocity weakening, likely due to the presence of high-pressure water, making it more susceptible to weakening. In this study, the antigorite gouge displayed velocity-strengthening friction characteristics across the entire temperature range. When the temperature exceeded 400 °C, the temperature-dependent variation of the velocity-dependent parameter ($a - b$) showed a trend consistent with the results of Takahashi et al. (2011) and Okazaki and Katayama (2015), indicating significant temperature weakening. This phenomenon may be associated with the dehydration reaction of antigorite. However, this reaction was not intense, and the microstructural analysis did not reveal significant forsterite formation (Figs. 6 and 7) (Takahashi et al., 2011). Consequently, the trace amounts of forsterite formed in this experiment had a limited effect on friction strength and a weak impact on the frictional sliding stability.

Additionally, when comparing the frictional sliding stability of antigorite gouge under high pore fluid pressure conditions, it is observed that below 400 °C, the velocity dependence parameter ($a - b$) exhibits similar trends under both pore fluid pressure conditions. However, under the low pore fluid pressure conditions in this study, no velocity weakening phenomenon was observed at 300 °C. When the temperature exceeds 400 °C, the trend of ($a - b$) shows significant differences between the two pore fluid pressure conditions. Under high pore fluid pressure conditions, the direct response parameter a increases monotonically with temperature above 300 °C, rising from 0.0065 at 300 °C to 0.0262 at 500 °C, nearly tripling (Fig. 8). This enhanced velocity response indicates a significant increase in the rheology of the contact points (Nakatani, 2001; Rice et al., 2001). The microstructural deformation mechanism may involve multiple processes, including dislocation slip along the (001) plane of antigorite (Shao et al., 2021) or grain-boundary pressure solution (He et al., 2013; Liu and He, 2020), along with grain fracturing. However, Liu et al. (2023) observed only grain-boundary pressure solution, with no evidence of grain bending, suggesting that the pressure solution process is likely the main controlling mechanism for the rheological behavior of the contact points under these conditions. This suggests that the presence of high pore fluid pressure significantly enhances the rheology of the gouge.

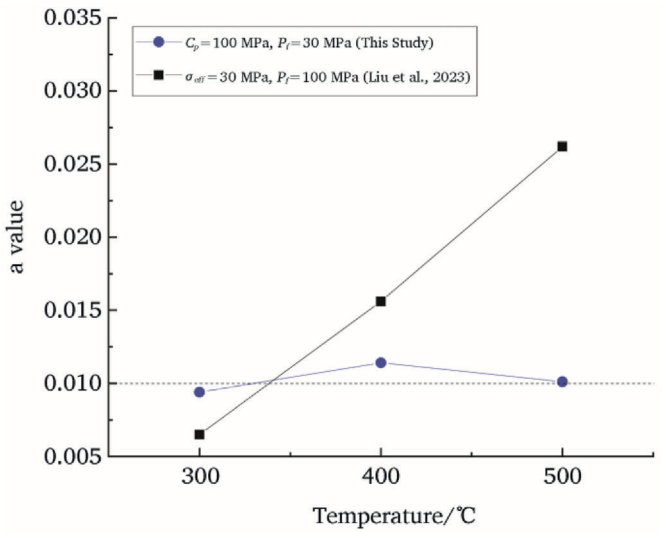

Fig. 8. The variation of the direct response parameter a with temperature (σ_{eff} is effective normal stress, C_p is confining pressure, P_f is pore fluid pressure).

Under low pore fluid pressure conditions, the direct response parameter a remains around 0.01 within the temperature range of 300–500 °C, first increasing and then decreasing with temperature. Specifically, it rises from 0.0094 at 300 °C to 0.0114 at 400 °C, then decreases to 0.0101 at 500 °C (Fig. 8). This trend suggests that the friction mechanism still dominates under these conditions, microstructural observations reveal pronounced grain-size reduction, indicating that the principal deformation mechanism is likely controlled by cataclastic flow rather than by significant viscous creep.

Accordingly, variations in pore-fluid pressure may exert a significant influence on the velocity dependence of frictional sliding in antigorite gouge. Under high pore fluid pressure conditions, increasing temperature enhances the rheology of the contact points, possibly controlled by a thermally activated mechanism. In contrast, under low pore fluid pressure conditions, the frictional sliding mechanism is mainly governed by fracturing flow, and the trend in a suggests that it remains within a friction-dominated regime.

5. Conclusions

Based on the rate-and-state dependent friction constitutive relations, this study conducted frictional sliding experiments under hydrothermal conditions to investigate the variation of the friction coefficient and sliding velocity dependence of antigorite gouge with temperature under low pore fluid pressure conditions. The experimental conditions were at a confining pressure of 100 MPa, a pore fluid pressure of 30 MPa, and the temperature range from 100 °C to 500 °C. To obtain the velocity dependence of antigorite gouge, different loading rates (1.0, 0.2, and 0.04 μm/s) were applied during the experiment. The main experimental results are as follows.

(1) In the temperature range of 100 °C–400 °C, the friction coefficient of antigorite gouge gradually decreases with increasing temperature, from 0.66 to 0.54, exhibiting a temperature weakening effect. However, above 400 °C, the friction coefficient increases, reaching 0.7 at 500 °C, exhibiting a temperature strengthening phenomenon.
(2) The study demonstrated that antigorite gouge exhibited velocity strengthening behavior across the entire experimental temperature range, suggesting stable sliding under these conditions. Microstructural analysis, including SEM and crystallochemical approaches, revealed that the deformation mechanisms of antigorite gouge evolve with temperature. At 200 °C, the deformation was primarily brittle, dominated by grain boundary sliding and micro-fracturing, while at 500 °C, plastic deformation mechanisms, such as dislocation glide along the basal planes, became active, leading to increased grain granulation.
(3) The impact of pore-fluid pressure was also a critical factor influencing the frictional behavior of antigorite. Under low pore-fluid pressure (30 MPa), the friction coefficient showed a clear increase above 400 °C, associated with dehydration hardening. In contrast, under high pore-fluid pressure conditions, frictional weakening persisted at elevated temperatures due to the suppression of water release and hydrogen bond breakdown, demonstrating the important role of pore-fluid pressure in regulating the frictional stability of antigorite gouge.

In conclusion, this study provides a comprehensive understanding of the temperature and pore-fluid pressure dependence of antigorite gouge's frictional properties, shedding light on its role in subduction-zone dynamics, particularly in the context of slow-slip events and fault stability. Further investigations into the mechanisms of water migration, dislocation behavior, and the influence of varying pore-fluid pressures are necessary to fully comprehend the complex frictional behavior of antigorite gouge under tectonic conditions.

CRediT authorship contribution statement

Shimin Liu: Writing – review & editing, Writing – original draft, Methodology, Funding acquisition, Data curation. **Mengke An:** Writing – review & editing, Supervision, Methodology, Conceptualization. **Wenhao Dai:** Supervision, Investigation, Conceptualization. **Huiru Lei:** Methodology, Investigation, Formal analysis. **Lei Zhang:** Writing – review & editing, Supervision, Methodology, Funding acquisition, Conceptualization. **Yongsheng Zhou:** Supervision, Conceptualization. **Zekang Yang:** Investigation.

Declaration of competing interest

The authors declare that they have no conflict of interest.

Acknowledgments

We give special thanks to Xi Ma for his help in using the SEM system for microstructural observations. We thank Wenming Yao for maintaining the testing system, especially for building the furnace. This research is supported by the Langfang Science and Technology Research and Development Program (Grants No. 2024013158), funded by the Langfang Science and Technology Bureau and the National Natural Science Foundation of China (Grants No. 42494862).

References

Auzende, A.L., Guillot, S., Devouard, B., Baronnet, A., 2006. Serpentinites in an Alpine convergent setting: effects of metamorphic grade and deformation on microstructures. Eur. J. Mineral 18 (1), 21–33.
Brune, J.N., Henyey, T.L., Roy, R.F., 1969. Heat flow, stress and rate of slip along the San Andreas fault, California. J. Geophys. Res. 74, 3821–3827.
Christensen, N.I., 1972. The abundance of serpentinites in the oceanic crust. J. Geol. 80 (6), 709–719.
Chernak, L.J., Hirth, G., 2010. Deformation of antigorite serpentinite at high temperature and pressure. Earth Planet Sci. Lett. 296 (1–2), 23–33.
Dietz, R.S., 1963. Alpine serpentines as oceanic rind fragments. Geology Society of America Bulletin 74 (7), 947–952.
Dengo, C.A., Logan, J.M., 1981. Implications of the mechanical and frictional behavior of serpentinite to seismogenic faulting. J. Geophys. Res. 86 (B11).
Dieterich, J.H., 1979. Modeling of rock friction: 1. Experimental results and constitutive equations. J. Geophys. Res. 84, 2161–2168.
Dieterich, J.H., Linker, M.L., 1992. Fault stability under conditions of variable normal stress. Geophys. Res. Lett. 19 (16), 1691–1694.
Evans, B.W., 1976. Stability of chrysotile and antigorite in the serpentinite multisystem. Schweizerische Mineralogische und Petrographische Mitteilungen 56 (1), 79–93.
Evans, B.W., 2004. The serpentinite multisystem revisited: chrysotile is metastable. Int. Geol. Rev. 46 (6), 479–506.

French, M.E., Hirth, G., Okazaki, K., 2019. Fracture-induced pore fluid pressure weakening and dehydration of serpentinite. Tectonophysics 767, 228168.
Hacker, Bradley R., 2003. Subduction factory 2. Are intermediate-depth earthquakes in subducting slabs linked to metamorphic dehydration reactions? J. Geophys. Res. Solid Earth 108 (B1), 2030.
Hilairet, N., Reynard, B., Wang, Y.B., Daniel, I., Merkel, S., Nishiyama, N., Petitgirard, 2007. High-pressure creep of serpentine, interseismic deformation, and initiation of subduction. Science 318 (5858), 1910–1913.
Hilairet, N., Reynard, B., 2009. Stability and dynamics of serpentinite layer in subduction zone. Tectonophysics 465 (1–4), 24–29.
He, C., Yao, W., Wang, Z., Zhou, Y., 2006. Strength and stability of frictional sliding of gabbro gouge at elevated temperatures. Tectonophysics 427 (1–4), 217–229.
He, C., Wang, Z., Yao, W., 2007. Frictional sliding of gabbro gouge under hydrothermal conditions. Tectonophysics 445 (3–4), 353–362.
He, C., Luo, L., Hao, Q., Zhou, Y., 2013. Velocity-weakening behavior of plagioclase and pyroxene gouges and stabilizing effect of small amounts of quartz under hydrothermal conditions. J. Geophys. Res. 118 (7), 3408–3430.
Jung, H., Green, H.W., 2004. Experimental faulting of serpentinite during dehydration: implications for earthquakes, seismic low-velocity zones, and anomalous hypocenter distributions in subduction zones. Int. Geol. Rev. 46 (12), 108–1102.
Jung, H., 2011. Seismic anisotropy produced by serpentine inmantle wedge. Earth Planet Sci. Lett. 307 (3–4), 535–543.
Kawakatsu, H., Watada, S., 2007. Seismic evidence for deep-water transportation in the mantle. Science 316 (5830), 1468–1471.
Katayama, I., Hirauchi, K.I., Michibayashi, K., Ando, J., 2009. Trench-parallel anisotropy produced by serpentine deformation in the hydrated mantle wedge. Nature 461 (7267), 1114–1117.
Liu, S., Zhang, L., He, C., 2023. Frictional properties of antigorite under high pore-fluid pressure and implications for slow-slip events in subduction zones. Chin. J. Geophys. 66 (4), 1334–1347.
Li, J., Guo, S., Yang, G., Qi, S., 2025. The influence of faults on adjacent rock mechanical behavior and acoustic emission characteristics: A case study of the xianshuihe fault zone. Rock Mech. Bull. 4 (4), 100210.
Liu, Y., He, C., 2020. Friction properties of hornblende and implications for slow-slip events in subduction zones. Tectonophysics 796.
Moore, D.E., Lockner, D.A., Ma, S.L., Summers, R., Byerlee, J.D., 1997. Strengths of serpentinite gouges at elevated temperatures. J. Geophys. Res. Solid Earth 102 (B7), 14787–14801.
Moore, D.E., Lockner, D.A., 2007. Comparative deformation behavior of minerals in serpentinized ultramafic rock: application to the slab-mantle interface in subduction zones. Int. Geol. Rev. 49 (5), 401–415.
Moore, D.E., Lockner, D.A., 2013. Chemical controls on fault behavior: weakening of serpentinite sheared against quartz-bearing rocks and its significance for fault creep in the San andreas system. J. Geophys. Res. Solid Earth 118 (5), 2558–2570.
Morrow, C.A., Moore, D.E., Lockner, D.A., 2000. The effect of mineral bond strength and adsorbed water on fault gouge frictional strength. Geophys. Res. Lett. 27 (6), 815–818.
Nakatani, M., 2001. Conceptual and physical clarification of rate and state friction: frictional sliding as a thermally activated rheology. J. Geophys. Res. 106, 13347–13380.
Okazaki, K., Katayama, I., 2015. Slow stick slip of antigorite serpentinite under hydrothermal conditions as a possible mechanism for slow earthquakes. Geophys. Res. Lett. 42 (4), 1099–1104.
Peacock, S.A., 1990. Fluid processes in subduction zones. Science 248 (4953), 329–337.
Peacock, S.M., 1993. Large-scale hydration of the lithosphere above subducting slabs. Chem. Geol. 108 (1–4), 49–59.
Perrillat, J.P., Daniel, I., Koga, K.T., Reynard, B., Cardon, H., Crichton, W.A., 2005. Kinetics of antigorite dehydration: a real-time X-ray diffraction study. Earth Planet Sci. Lett. 236 (3–4), 899–913.
Raleigh, C.B., Paterson, M.S., 1965. Experimental deformation of serpentinite and its tectonic implications. J. Geophys. Res. 70 (16), 3965–3985.
Ruina, A., 1983. Slip instability and state variable friction laws. J. Geophys. Res. Solid Earth 88 (B12), 10359–10370.
Reinen, L.A., Weeks, J.D., Tullis, T.E., 1991. The frictional behavior of serpentinite: implications for aseismic creep on shallow crustal faults. Geophys. Res. Lett. 18 (10), 1921–1924.
Reinen, L.A., 1994. The frictional behavior of lizardite and antigorite serpentinites: experiments, constitutive models, and implications for natural faults. Pure Appl. Geophys. 143 (1–3), 317–358.
Rice, J.R., Lapusta, N., Ranjith, K., 2001. Rate and state dependent friction and the stability of sliding between elastically deformable solids. J. Mech. Phys. Solid. 49 (9), 1865–1898.
Schwartz, S., Guillot, S., Reynard, B., Reynard, B., Lafay, R., Debret, B., Nicollet, C., Lanari, P., Auzende, A.L., 2013. Pressure-temperature estimates of the lizardite/antigorite transition in high pressure serpentinites. Lithos 178 (15), 197–210.
Shao, T.B., Zhou, Y.S., Song, M.S., Ma, X., Zhang, L., Yao, W., Dang, J., Li, J., 2021. Deformation of antigorite and its geological implications. J. Geophys. Res. Solid Earth 126 (6), e2021JB021650.
Tse, S.T., Rice, J.R., 1986. Crustal earthquake instability in relationship to the depth variation of frictional slip properties. J. Geophys. Res. 91 (B9), 9452–9472.
Takahashi, M., Uehara, S.I., Mizoguchi, K., Shimizu, I., Okazaki, K., Masuda, K., 2011. On the transient response of serpentine (antigorite) gouge to stepwise changes in slip velocity under high-temperature conditions. J. Geophys. Res. 116 (B10), B10405.
Viti, C., Collettini, C., Tesei, T., Tarling, M.S., Smith, S.A.F., 2018. Deformation processes, textural evolution and weakening in retrograde serpentinites. Minerals 8, 241.
Wunder, B., Schreyer, W., 1997. Antigorite: High-pressure stability in the system MgO-SiO_2-H_2O (MSH). Lithos 41 (1), 213–227.
Zoback, M.D., 1987. New evidence for the state of stress on the san andreas fault system. Science 238, 1105–1111.